

Stationary entanglement of a levitated oscillator with an optical field

Q. Deplano,^{1,2,*} A. Pontin,^{3,*} F. Marino,^{3,2} and F. Marin^{1,4,2,3,†}

¹*Dipartimento di Fisica e Astronomia, Università di Firenze,
via Sansone 1, I-50019 Sesto Fiorentino (FI), Italy*

²*INFN, Sezione di Firenze, via Sansone 1, I-50019 Sesto Fiorentino (FI), Italy*

³*CNR-INO, largo Enrico Fermi 6, I-50125 Firenze, Italy*

⁴*European Laboratory for Non-Linear Spectroscopy (LENS),
via Carrara 1, I-50019 Sesto Fiorentino (FI), Italy*

(Dated: February 4, 2026)

We report the generation of quantum entanglement between the center-of-mass motion of a levitated nanosphere, coupled by coherent scattering to an optical cavity mode, and the electromagnetic field. Using heterodyne detection, we reconstruct the full set of optical-mechanical correlations and observe a violation of separability bounds between the mechanical degrees of freedom and the propagating optical mode. Thus, we demonstrate the ability to distribute nonclassical correlations beyond the interaction region. Our results are obtained at room temperature and are robust over a broad range of detunings set by the cavity linewidth. These findings establish levitated optomechanical systems as a promising platform for macroscopic quantum optics and for future tests of fundamental physics.

Entanglement lies at the heart of quantum mechanics [1, 2], and the ability to observe and control it in macroscopic systems is a crucial goal with far-reaching implications for quantum technologies and for exploring the foundations of quantum physics. Optomechanical platforms have enabled exquisite control over mechanical motion, leading to milestones such as the preparation of deeply nonclassical mechanical states [3, 4]. Entanglement between mechanical oscillators [5–9], between a drum oscillator and a microwave [10], and between nano-oscillators and single photons [11], has been demonstrated in ultra-cryogenic environments. While optomechanical interaction can entangle distinct optical fields [12, 13], realizing stationary entanglement between mechanical motion and the light, eventually propagating beyond the interaction region, has so far remained elusive, despite long-standing theoretical proposals [14–19]. The generation of such light-matter entanglement is of particular interest because it provides a natural interface between stationary and flying quantum degrees of freedom such that the non-local correlations can propagate in space. Among optomechanical platforms, levitated systems have recently emerged as a particularly attractive approach [20], combining strong light-matter interactions [21, 22] with an

exceptional degree of isolation from the environment [23, 24]. The center-of-mass oscillatory motion of dielectric nanospheres confined in optical tweezers has indeed been brought into the one- and two-dimensional quantum regime [25–31]. Here, we achieve a further milestone by showing correlations that violate separability bounds between the mechanical and the optical field degrees of freedom, involving both the light inside an optical cavity, and the propagating outgoing wave.

Experimental procedure - We load a 100 nm diameter silica sphere in an optical tweezer [32] created by two laser fields (denoted A and B) at 1064 nm, superposed inside an optical fiber with identical linear polarization and a power ratio of 3:1. Owing to a slight ellipticity of the focused beam, with the major axis aligned along the polarization direction (see inset in Fig. 1 b)), the motion in the transverse plane of the tweezer exhibits two distinct mechanical frequencies, $\Omega_x/2\pi = 110.6$ kHz and $\Omega_y/2\pi = 98.4$ kHz. The nanosphere is placed at the center of an optical cavity whose axis is orthogonal to that of the tweezer. Both trapping lasers are phase locked to an auxiliary laser that is frequency stabilized to a cavity resonance, enabling precise control of their detunings $\Delta_{A,B}$ from two longitudinal cavity modes separated by twice the cavity free spectral range (FSR = 3.07 GHz). The configuration is shown in Fig. 1 a). Light scattered from the tweezer fields populates the two cavity modes, thereby coupling the particle's motion to the intracavity fields via coherent scattering [21, 33–35]. A simplified experimental scheme is shown in Fig. 1 b).

When the nanosphere is located near a node of the cavity standing wave, the dominant optomechanical coupling involves motion along the cavity axis (the bright mechanical mode [36–38], with eigenfrequency $\Omega_b \simeq (\Omega_x + \Omega_y)/2$). The red-detuned field A directly cools this bright mode. Because the polarization axis is oriented at $\sim 45^\circ$ relative to the cavity axis, both transverse motional degrees of freedom are cooled. As a consequence, the direction orthogonal to the cavity axis (dark mode), even if it is not directly coupled to the cavity field, undergoes efficient sympathetic cooling [28, 30, 37]. Operating in the resolved-sidebands regime, where the cavity decay rate κ is smaller than Ω_b , optimal cooling is achieved for detuning $-\Delta_A \simeq \Omega_b$. In this regime, the optomechanical interaction is well described by a beam-splitter Hamiltonian $\hbar g_A (\hat{a}_A^\dagger \hat{b} + \hat{a}_A \hat{b}^\dagger)$ (g_A is the coupling rate, \hat{a}_A and \hat{b} are the annihilation operators of the optical and mechanical modes, respectively).

The field outgoing the cavity for each optical mode $\alpha = (A, B)$ is

$$a_\alpha^{out} = \sqrt{\eta} \left(e^{i\phi_\alpha} a_\alpha^{in} + i g_\alpha \sqrt{\kappa} \chi_\alpha x_b \right) + \sqrt{1-\eta} a_\alpha^v \quad (1)$$

where a_α^{in} denotes the vacuum input field, ϕ_α a frequency-dependent phase, χ_α the cavity susceptibility, and a_α^v the vacuum field associated with the overall propagation and detection losses, quantified by the efficiency η . This expression highlights that, in addition to providing cooling and

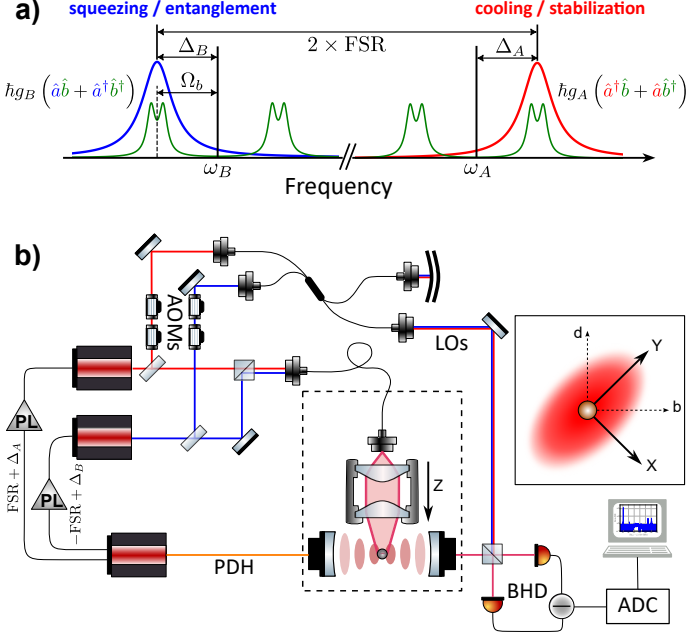


FIG. 1. **Experimental configuration.** The motion of a levitated nanoparticle is coupled to the field of an optical cavity via coherent scattering. The confining potential is obtained by overlapping in the optical tweezer two fields, A and B , with different frequencies. This enables simultaneous driving of the cavity on opposite sides of its resonances, with detunings Δ_A (red) and Δ_B (blue): the former cools and stabilizes the motion, while the latter generates entanglement between the mechanical and optical subsystems. **a)** The detuning of the A and B fields is set with respect to different longitudinal modes separated by two free spectral ranges (FSR) at a value close to the mechanical bright mode frequency Ω_b . **b)** This is achieved by phase locking (PL) both trapping lasers to an auxiliary laser, frequency stabilized to a cavity resonance using a Pound-Drever-Hall (PDH) locking scheme. The cavity output fields are measured in a heterodyne configuration using the same balanced detection (BHD). We use two different local oscillators frequencies, detuned by 1.4 MHz and 2.0 MHz with respect to the corresponding trapping fields by means of acousto-optical modulators (AOM). The heterodyne signals are recorded after a high-resolution analog-to-digital converter (ADC). The inset depicts the beam shape of the tweezer (polarized along Y) in the transverse plane. The label "b" ("d") refers to "bright" ("dark") and corresponds to the direction along (orthogonal to) the cavity axis. Measurements are performed in UHV environment, at a pressure of $\simeq 3.5 \times 10^{-8}$ mbar.

stabilization, the outgoing field A constitutes a meter for the bright mode displacement x_b (here normalized to its zero-point fluctuations).

The B field, blue detuned with respect to the nearest cavity resonance, plays the central role in the experiment. When $\Delta_B \simeq \Omega_b$, its interaction with the nanosphere motion is well described by a two-mode squeezing Hamiltonian $\hbar g_B (\hat{a}_B\hat{b} + \hat{a}_B^\dagger\hat{b}^\dagger)$, which generates entanglement between the electromagnetic field and the bright mechanical mode. These quantum correlations are preserved

in the field propagating out of the cavity. Inside the cavity, the electromagnetic field modes are uniquely determined by the boundary conditions. In contrast, propagating modes allow for a certain degree of arbitrariness in their definition. We may introduce a mode annihilation operator as

$$a_\xi = \int_{-\infty}^{\infty} \xi(-t) a^{out}(t) dt = \int_{-\infty}^{\infty} \xi(\omega) a^{out}(\omega) \frac{d\omega}{2\pi} \quad (2)$$

where the envelope function $\xi(t)$ is normalized according to $\int_{-\infty}^{\infty} |\xi(t)|^2 dt = 1$ [17]. The function $\xi(\omega)$ denotes the Fourier transform defined as $\xi(\omega) \equiv \mathcal{F}[\xi(t)] = \int_{-\infty}^{\infty} \xi(t) e^{i\omega t} dt$. It can be shown that a_ξ obeys the canonical bosonic commutation relations $[a_\xi, a_\xi^\dagger] = 1$. The corresponding mode quadratures are defined as $Q_\xi = a_\xi + a_\xi^\dagger$ and $P_\xi = i(a_\xi^\dagger - a_\xi)$.

In the following we will consider propagating optical modes defined by a flat spectral window centered at $-\Omega_b$, i.e., by $\xi(\omega) = 1/\sqrt{2\pi\Gamma_\xi}$ for $(-\Omega_b - \Gamma_\xi/2) < \omega < (-\Omega_b + \Gamma_\xi/2)$, and $\xi(\Omega) = 0$ elsewhere.

Data analysis and modeling - Direct access to intracavity operators is not available, but information about the quantum state of the system is encoded in the fields propagating out of the cavity. We retrieve this information using heterodyne detection. To this purpose, two local oscillators, with different detuning $\Omega_{LO}^A/2\pi = 1.4$ MHz and $\Omega_{LO}^B/2\pi = 2.0$ MHz from the respective signal fields, are overlapped and directed onto a single balanced detection that probes the light transmitted by the cavity. The heterodyne photocurrent operator is $i_{het} = \alpha_{LO}^* a^{out} e^{i\Omega_{LO} t} + \alpha_{LO} a^{out\dagger} e^{-i\Omega_{LO} t}$ where α_{LO} is the local oscillator field [39]. i_{het} is Hermitian and satisfies $i_{het}(-\omega) = (i_{het}(\omega))^\dagger$.

From the heterodyne signal we experimentally reconstruct the spectral correlation matrix $\mathbf{A} = \langle a_i a_j \rangle$ of the output fields ladder operators $\mathbf{a} = (a_A^{out}, a_A^{out\dagger}, a_B^{out}, a_B^{out\dagger})$ where $O^\dagger(\omega) = \mathcal{F}[O^\dagger(t)]$ [18]. To this end, a phase-sensitive analysis is required. For this reason the nanosphere is positioned at a small but finite distance from nodes of both A and B intracavity stationary waves, so that weak coherent signals are generated in a_α^{out} providing a stable phase reference and enabling consistent determination of the field quadratures across the full data set.

The heterodyne signal is continuously acquired and the recorded data are segmented into 10 ms long intervals. For each interval, the Fourier transform of the heterodyne signal, $v(\omega)$, is computed and assembled into the four-dimensional data vector $\mathbf{v}(\Omega) = (v(\Omega_{LO}^A + \Omega), v^*(\Omega_{LO}^A - \Omega), v(\Omega_{LO}^B + \Omega), v^*(\Omega_{LO}^B - \Omega))$. From this vector, compensated for the frequency-dependent argument of the electronic response, we evaluate the spectral correlation matrix \mathbf{C} defined as $C_{ij} = \langle v_i(\Omega) v_j^*(-\Omega) \rangle$ where $\langle \cdot \rangle$ denotes ensemble averaging. Calibration of \mathbf{C} to the standard quantum noise level of fields A and B (obtained by blocking the signal path in the heterodyne detection) is followed by

subtraction of electronic noise. This procedure transforms \mathbf{C} into a new matrix $\mathbf{A}^\phi = \mathbf{R}\mathbf{A}\mathbf{R}^T$ where \mathbf{R} is a constant matrix accounting for the phases, ϕ_A and ϕ_B , of the two detected coherent components with respect to the intracavity fields which define the reference phase in the modeling.

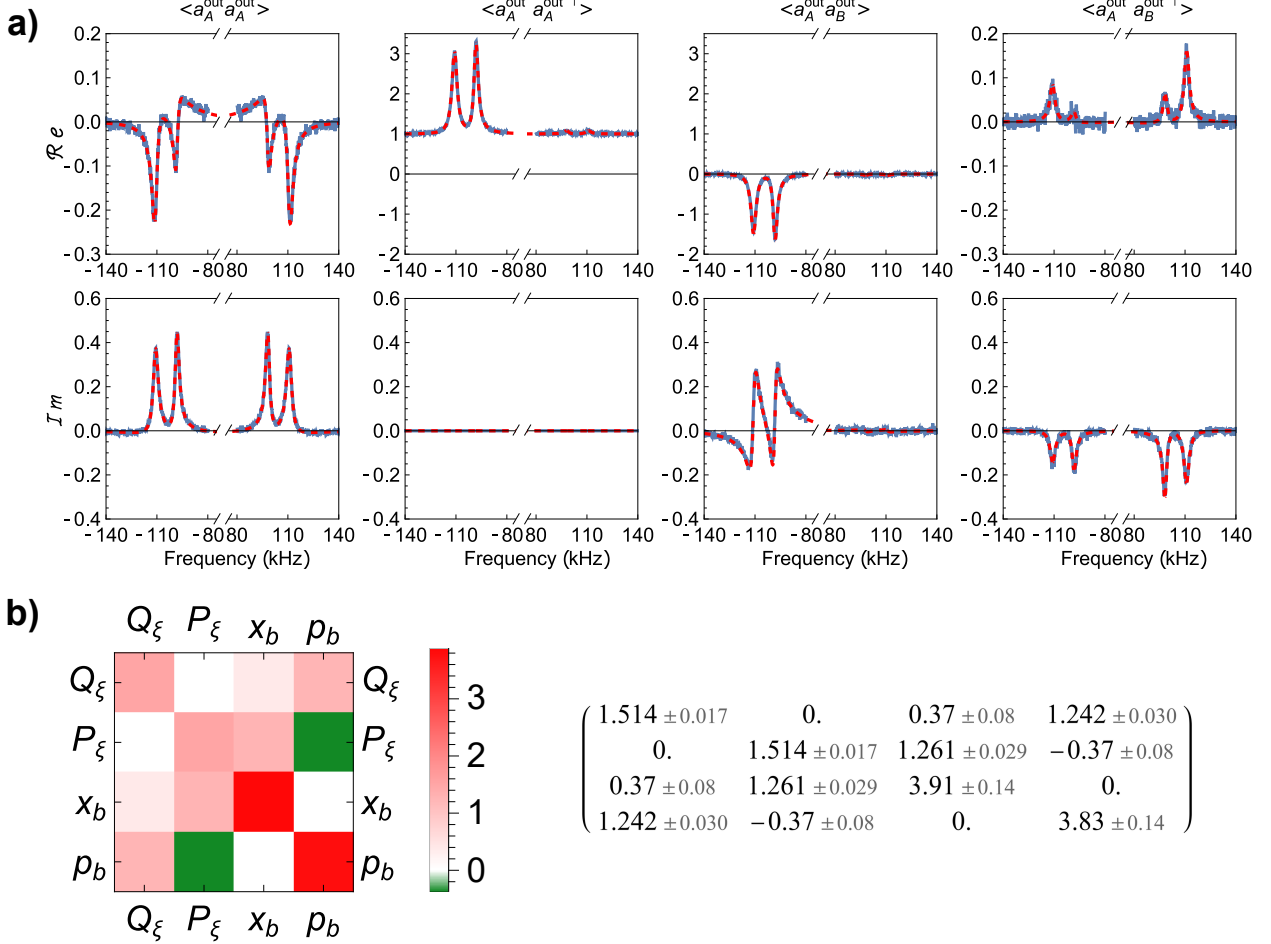


FIG. 2. **Optomechanical correlations.** **a)** First row of the complex-valued spectral matrix \mathbf{A} , shown around the bright mode sidebands, along with the fitted theoretical model (dashed-red line). Each column in the figure represent the real (top) and imaginary (bottom) part of \mathbf{A} . **b)** 2D portrayal of the covariance matrix \mathbf{V} fully characterizing the optical-mechanical Gaussian state, and corresponding numerical values. The estimated dynamical parameters for this dataset are $\Omega_b/2\pi = 106 \pm 0.1$ kHz, $g_A/2\pi = 11.7 \pm 0.2$ kHz, $g_B/2\pi = 6.3 \pm 0.1$ kHz. The heating rates are $\Gamma_x/2\pi = 3.00 \pm 0.05$ kHz and $\Gamma_y/2\pi = 2.67 \pm 0.05$ kHz. All quoted errors indicate one SD of ~ 10 independent samples.

The spectral matrix \mathbf{A} contains all the information that can be extracted from the two outgoing fields. Owing to intrinsic symmetries, it comprises 16 different real-valued, frequency-dependent functions. For all intents and purposes, the elements $A_{1,2}^\phi$ and $A_{3,4}^\phi$ represent the usual heterodyne power spectral density (PSD) of the fields A and B , respectively. These are fitted simultaneously

to the optomechanical model to extract the system parameters, namely, the pairs of mechanical bare frequencies, heating rates, and optomechanical coupling rates. Independent measurements provide $\kappa/2\pi = 58 \pm 0.6$ kHz and $\eta = 0.283 \pm 0.006$. The full \mathbf{A}^ϕ matrix is then fitted to the model to determine ϕ_A and ϕ_B . Representative examples of elements of \mathbf{A} are shown in Fig. 2 a) around the bright mode sidebands, along with the respective fitting curves.

The close agreement between the experimental data and the curves produced by the optomechanical model over the entire spectral matrix indicates a precise quantitative understanding of the system. This enables us to employ the same model, with the fitted parameters, to compute the covariance matrix \mathbf{V} describing the joint state of the bright mechanical mode and the propagating field mode B . The matrix elements are defined as $V_{ij} = 0.5\langle\{\mathbf{u}_i, \mathbf{u}_j\}\rangle$, where $\mathbf{u} = (Q_\xi, P_\xi, x_b, p_b)$. Here x_b and p_b denote the position and momentum of the bright mode normalized to their respective zero-point fluctuations, and $\{\cdot, \cdot\}$ indicates the anti-commutator.

We return to this method for evaluating \mathbf{V} below, but first consider a more direct route that fully exploits the matrix \mathbf{A} , which provides a complete description of the correlations between the output fields A and B . This is achieved by applying a suitable linear transformation and integrating over frequency. The transformation matrix incorporates the envelope function $\xi(\omega)$, while the mechanical observables are reconstructed from field A by inverting Eq. 1. Explicitly, we define $x_{meas} = \frac{a_A^{out}}{i\sqrt{\eta\kappa}g_A\chi_A}$, $p_{meas} = i\frac{\omega}{\Omega_b}x_{meas}$, and consider them as a reliable measurement of the true mechanical quadratures, x_b and p_b , to evaluate \mathbf{V} . Importantly, the noise properties and correlations that quantify the quantum character of the system emerge directly from the processed data, instead of being deduced from the fit of the model. A representative covariance matrix obtained with this method is shown in Fig. 2 b).

Results & discussion - The entanglement between the optical and mechanical subsystems is quantified by the smallest symplectic eigenvalue, ν_- , of the partially transposed covariance matrix [40, 41]. With our normalization, $\nu_- = 1$ if the two oscillators are in uncorrelated vacuum states, and the presence of entanglement is signaled by $\nu_- < 1$. Fig. 3 reports the values of ν_- calculated from the covariance matrix \mathbf{V} directly reconstructed through \mathbf{A} , as a function of the width Γ_ξ of $\xi(\omega)$. Entanglement emerges when the bandwidth Γ_ξ of the optical mode becomes sufficiently large to encompass the full spectral response of the mechanical bright mode [17], characterized by two peaks at $\sim \Omega_x$ and $\sim \Omega_y$ broadened by optomechanical interaction. The minimum value of ν_- , corresponding to maximal entanglement, is achieved around $\Gamma_\xi/2\pi = 40$ kHz and reaches $\nu_- = 0.931 \pm 0.015$. Here, the quoted statistical uncertainty represents one standard deviation obtained from multiple measurements, while an additional systematic uncertainty of ± 0.02 arises

from independent estimates of η and κ .

Entanglement is commonly quantified by the logarithmic negativity E_N , defined as $E_N = \max\{0, -\log_2(\nu_-)\}$ [42, 43]. At its maximum, we obtain $E_N = 0.10 \pm 0.03$, including both the statistical and the systematic uncertainty.

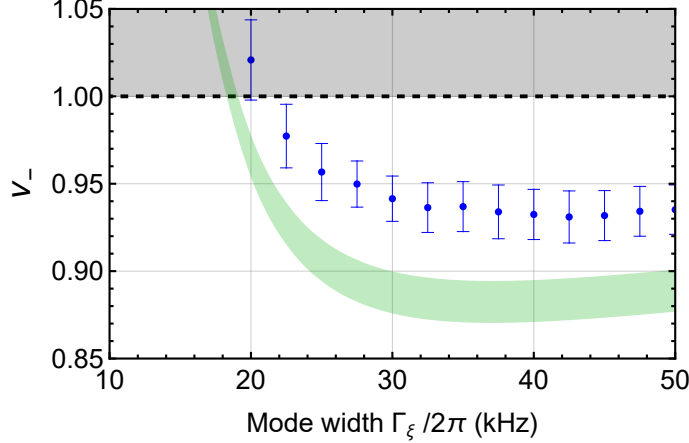


FIG. 3. Optimization of the optical mode width. The smallest symplectic eigenvalue ν_- of the partially trasposed covariance matrix \mathbf{V} is plotted as a function of mode width Γ_ξ . The data points with error bars (indicating one SD over about 10 independent data acquisitions) are obtained from \mathbf{V} directly reconstructed from the experimental correlation matrix. The green shaded area derives from \mathbf{V} computed with our optomechanical model, using the parameters that best fit the heterodyne spectra. The width of this band reflects systematic uncertainties in the model parameters (mainly the efficiency η), with negligible contribution from statistical uncertainty. The gray shaded region highlights the threshold above which the mechanical and optical subsystems become separable.

Fig. 3 also reports the values of ν_- obtained by estimating \mathbf{V} from the full optomechanical model using all the fitted parameters, including the heating rates. The model reproduces the overall trend of the values extracted directly from the experimental covariance matrix, but consistently yields lower values of ν_- . We attribute this discrepancy to slow fluctuations of the system parameters during the acquisition of the full time series, most notably of the relative phases ϕ_A and ϕ_B , which are not fully captured by the stationary description. To mitigate these effects, the data analysis is restricted to time intervals over which the fitted parameters remain approximately constant. In practice, each independent estimate of the correlation matrix \mathbf{A} — and hence of the covariance matrix \mathbf{V} and the symplectic eigenvalue ν_- — is obtained by averaging over typically 2000 consecutive time windows of 10 ms. Residual parameter fluctuations during these 20 seconds segments nevertheless lead to an effective mixing of slightly different Gaussian states, which results in a reduction of the observable entanglement. As a consequence, the entanglement actually present

in the system is more faithfully captured by estimating \mathbf{V} through the optomechanical model evaluated with the fitted parameters, whereas the values of ν_- directly inferred from the data should be regarded as a conservative estimate of the entanglement that can be effectively harnessed under the present level of system stability.

We also notice that we have defined the optical mode using a rectangular spectral filter. Although convenient, this choice is not optimal. A suitably tailored spectral mode could maximize the fidelity between the optical and mechanical subsystems and thereby enhance the observable entanglement.

The results discussed so far were obtained for detunings satisfying $-\Delta_A \simeq \Delta_B \simeq \Omega_b$. This condition, however, is not essential, and a finite degree of entanglement is present even when it is relaxed. Indeed, we repeated the experiment while varying the detuning, keeping only the condition $-\Delta_A \simeq \Delta_B$. Fig. 4 shows the symplectic eigenvalue ν_- derived from the covariance matrix \mathbf{V} reconstructed directly from the measured correlation matrix \mathbf{A} , together with the corresponding values obtained by computing \mathbf{V} with the optomechanical model using parameters fitted to the same experimental data. Entanglement persists over a detuning range exceeding 40 kHz, consistent with the expectation that it is maintained within a bandwidth on the order of the cavity linewidth κ . This robustness implies that stable opto-mechanical entanglement can be achieved without fine control of the detuning.

An important and nontrivial question is whether entanglement is also present inside the cavity, between the intracavity mode of field B and the mechanical oscillator. This is reasonable but not obvious, since the intracavity field mode is uniquely determined by the cavity boundary conditions and cannot be tailored as in the case of the propagating field. Although intracavity observables cannot be accessed directly, the same optomechanical model that quantitatively reproduces the measured output correlations allows us to reconstruct the corresponding intracavity covariance matrix from the fitted parameters. The resulting symplectic eigenvalue ν_- , shown in Fig. 4 as a function of the detuning, confirms the presence of intracavity entanglement, albeit at a reduced level compared to that of the propagating mode. The minimum inferred value of ν_- for the intracavity variables is $\nu_- = 0.885 \pm 0.003$, corresponding to a logarithmic negativity of $E_N = 0.176 \pm 0.005$, while for the propagating optical mode the same dataset gives $\nu_- = 0.860 \pm 0.013$ ($E_N = 0.218 \pm 0.023$).

In conclusion, we have demonstrated the generation of quantum entanglement between the center-of-mass motion of a levitated nanosphere and an optical field, extending beyond the interaction region and persisting in the propagating wave. By combining coherent scattering in

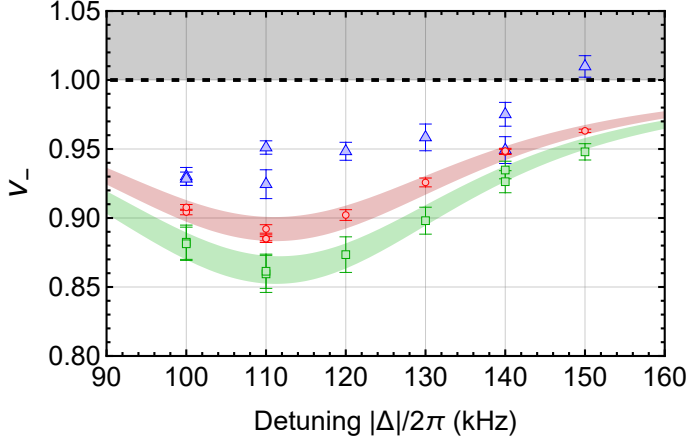


FIG. 4. **Symplectic eigenvalue versus cavity detuning.** Experimental data points shown by blue markers with error bars (SEM over about 10 independent data acquisitions) are obtained from the covariance matrix directly reconstructed from the measured correlations. Green markers are extracted instead from the same experimental data through the optomechanical model, using the parameters that best fit the heterodyne spectra. In this case the uncertainty is dominated by the systematic error on the detection efficiency η . In these measurements, we set $-\Delta_A \simeq \Delta_B = |\Delta|$. Intracavity entanglement is inferred from the symplectic eigenvalues associated to the covariance matrix calculated, within the same model and parameter set, for the joint state of the bright mode and the intracavity field (red points, with error bars again set by the systematic uncertainty on η). The green and red shaded regions are obtained by taking the extremal model predictions generated by the full set of parameters extracted from all data sets (at all detunings). These bands therefore illustrate the overall detuning dependence of the entanglement in our system.

an optical cavity with high efficiency heterodyne detection, we reconstruct the full set of optical–mechanical correlations and observe the violation of separability bounds under experimentally accessible conditions. These results establish levitated optomechanical systems as a versatile platform for achieving and exploiting light–matter entanglement. The ability to produce it at room temperature, without requiring ultra-cryogenic environments or fine-tuned parameters, represents a significant step toward practical macroscopic quantum technologies. A distinctive advantage of levitated systems is the availability of additional, weakly coupled mechanical degrees of freedom beyond center-of-mass motion, including rotational and librational modes [44–47]. Access to these additional mechanical degrees of freedom, combined with the prospect of trapping and simultaneously cooling multiple levitated nanospheres within a single optical cavity [48, 49], could enable the generation of multipartite and multimode entangled states mediated by a common optical field [50], while opening new avenues for scalable light–matter interfaces with enhanced sensitivity and control. More broadly, the combination of strong isolation, tunable interactions, and the ability

to distribute quantum correlations via propagating fields positions levitated optomechanics as a promising setting for future investigations of fundamental physics. In particular, these systems suggest a realistic path toward experimental tests of whether gravity can mediate quantum correlations, by enabling the preparation and control of nonclassical states of increasingly massive objects [51, 52]. Such experiments could provide new insights into the quantum nature of gravity and into possible modifications of quantum mechanics at macroscopic scales.

ACKNOWLEDGMENTS

The authors would like to acknowledge useful discussions with D. Vitali and P. F. Barker. We acknowledge financial support from PNRR MUR Project No. PE0000023-NQSTI and by the European Commission-EU under the Infrastructure I-PHOQS “Integrated Infrastructure Initiative in Photonic and Quantum Sciences ” [IR0000016, ID D2B8D520, CUP D2B8D520].

* These authors contributed equally

† Electronic mail: francesco.marin@unifi.it

- [1] A. Einstein, B. Podolsky, and N. Rosen, Can quantum-mechanical description of physical reality be considered complete?, *Phys. Rev.* **47**, 777 (1935).
- [2] E. Schrödinger, Discussion of probability relations between separated systems, *Mathematical Proceedings of the Cambridge Philosophical Society* **31**, 555–563 (1935).
- [3] P. Arrangoiz-Arriola, E. A. Wollack, Z. Wang, M. Pechal, W. Jiang, T. P. McKenna, J. D. Witmer, R. Van Laer, and A. H. Safavi-Naeini, Resolving the energy levels of a nanomechanical oscillator, *Nature* **571**, 537 (2019).
- [4] M. Bild, M. Fadel, Y. Yang, U. von Lüpke, P. Martin, A. Bruno, and Y. Chu, Schrödinger cat states of a 16-microgram mechanical oscillator, *Science* **380**, 274 (2023).
- [5] C. F. Ockeloen-Korppi, E. Damskägg, J.-M. Pirkkalainen, M. Asjad, A. A. Clerk, F. Massel, M. J. Woolley, and M. A. Sillanpää, Stabilized entanglement of massive mechanical oscillators, *Nature* **556**, 478 (2018).
- [6] R. Riedinger, A. Wallucks, I. Marinković, C. Löschnauer, M. Aspelmeyer, S. Hong, and S. Gröblacher, Remote quantum entanglement between two micromechanical oscillators, *Nature* **556**, 473 (2018).
- [7] S. Kotler, G. A. Peterson, E. Shojaaee, F. Lecocq, K. Cicak, A. Kwiatkowski, S. Geller, S. Glancy, E. Knill, R. W. Simmonds, J. Aumentado, and J. D. Teufel, Direct observation of deterministic macroscopic entanglement, *Science* **372**, 622 (2021), <https://www.science.org/doi/pdf/10.1126/science.abf2998>.

[8] L. M. de Lépinay, C. F. Ockeloen-Korppi, M. J. Woolley, and M. A. Sillanpää, Quantum mechanics-free subsystem with mechanical oscillators, *Science* **372**, 625 (2021), <https://www.science.org/doi/pdf/10.1126/science.abf5389>.

[9] E. A. Wollack, A. Y. Cleland, R. G. Gruenke, Z. Wang, P. Arrangoiz-Arriola, and A. H. Safavi-Naeini, Quantum state preparation and tomography of entangled mechanical resonators, *Nature* **604**, 463 (2022).

[10] T. A. Palomaki, J. D. Teufel, R. W. Simmonds, and K. W. Lehnert, Entangling mechanical motion with microwave fields, *Science* **342**, 710 (2013).

[11] I. Marinković, A. Wallucks, R. Riedinger, S. Hong, M. Aspelmeyer, and S. Gröblacher, Optomechanical bell test, *Phys. Rev. Lett.* **121**, 220404 (2018).

[12] S. Barzanjeh, E. S. Redchenko, M. Peruzzo, M. Wulf, D. P. Lewis, G. Arnold, and J. M. Fink, Stationary entangled radiation from micromechanical motion, *Nature* **570**, 480 (2019).

[13] J. Chen, M. Rossi, D. Mason, and A. Schliesser, Entanglement of propagating optical modes via a mechanical interface, *Nature Communications* **11**, 943 (2020).

[14] S. Bose, K. Jacobs, and P. L. Knight, Preparation of nonclassical states in cavities with a moving mirror, *Physical Review A* **56**, 4175–4186 (1997).

[15] D. Vitali, S. Gigan, A. Ferreira, H. R. Böhm, P. Tombesi, A. Guerreiro, V. Vedral, A. Zeilinger, and M. Aspelmeyer, Optomechanical entanglement between a movable mirror and a cavity field, *Phys. Rev. Lett.* **98**, 030405 (2007).

[16] M. Paternostro, D. Vitali, S. Gigan, M. S. Kim, C. Brukner, J. Eisert, and M. Aspelmeyer, Creating and probing multipartite macroscopic entanglement with light, *Phys. Rev. Lett.* **99**, 250401 (2007).

[17] C. Genes, A. Mari, P. Tombesi, and D. Vitali, Robust entanglement of a micromechanical resonator with output optical fields, *Phys. Rev. A* **78**, 032316 (2008).

[18] S. Zippilli, G. D. Giuseppe, and D. Vitali, Entanglement and squeezing of continuous-wave stationary light, *New Journal of Physics* **17**, 043025 (2015).

[19] C. Gut, K. Winkler, J. Hoelscher-Obermaier, S. G. Hofer, R. M. Nia, N. Walk, A. Steffens, J. Eisert, W. Wieczorek, J. A. Slater, M. Aspelmeyer, and K. Hammerer, Stationary optomechanical entanglement between a mechanical oscillator and its measurement apparatus, *Phys. Rev. Res.* **2**, 033244 (2020).

[20] C. Gonzalez-Ballester, M. Aspelmeyer, L. Novotny, R. Quidant, and O. Romero-Isart, Levitodynamics: Levitation and control of microscopic objects in vacuum, *Science* **374**, eabg3027 (2021), <https://www.science.org/doi/pdf/10.1126/science.abg3027>.

[21] A. de los Ríos Sommer, N. Meyer, and R. Quidant, Strong optomechanical coupling at room temperature by coherent scattering, *Nature Communications* **12**, 276 (2021).

[22] A. Ranfagni, P. Vezio, M. Calamai, A. Chowdhury, F. Marino, and F. Marin, Vectorial polaritons in the quantum motion of a levitated nanosphere, *Nature Physics* **17**, 1120 (2021).

[23] A. Pontin, N. P. Bullier, M. Toroš, and P. F. Barker, Ultranarrow-linewidth levitated nano-oscillator for testing dissipative wave-function collapse, *Phys. Rev. Research* **2**, 023349 (2020).

[24] L. Dania, D. S. Bykov, F. Goschin, M. Teller, A. Kassid, and T. E. Northup, Ultrahigh quality factor of a levitated nanomechanical oscillator, *Phys. Rev. Lett.* **132**, 133602 (2024).

[25] U. Delić, M. Reisenbauer, K. Dare, D. Grass, V. Vuletić, N. Kiesel, and M. Aspelmeyer, Cooling of a levitated nanoparticle to the motional quantum ground state, *Science* **367**, 892 (2020), <https://science.sciencemag.org/content/367/6480/892.full.pdf>.

[26] L. Magrini, P. Rosenzweig, C. Bach, A. Deutschmann-Olek, S. G. Hofer, S. Hong, N. Kiesel, A. Kugi, and M. Aspelmeyer, Real-time optimal quantum control of mechanical motion at room temperature, *Nature* **595**, 373 (2021).

[27] F. Tebbenjohanns, M. L. Mattana, M. Rossi, M. Frimmer, and L. Novotny, Quantum control of a nanoparticle optically levitated in cryogenic free space, *Nature* **595**, 378 (2021).

[28] A. Ranfagni, K. Børkje, F. Marino, and F. Marin, Two-dimensional quantum motion of a levitated nanosphere, *Phys. Rev. Research* **4**, 033051 (2022).

[29] J. Piotrowski, D. Windey, J. Vijayan, C. Gonzalez-Ballester, A. de los Ríos Sommer, N. Meyer, R. Quidant, O. Romero-Isart, R. Reimann, and L. Novotny, Simultaneous ground-state cooling of two mechanical modes of a levitated nanoparticle, *Nature Physics* **19**, 1009 (2023).

[30] Q. Deplano, A. Pontin, A. Ranfagni, F. Marino, and F. Marin, High purity two-dimensional levitated mechanical oscillator, *Nature Communications* **16**, 4215 (2025).

[31] M. Kamba, N. Hara, and K. Aikawa, Quantum squeezing of a levitated nanomechanical oscillator, *Science* **389**, 1225 (2025), <https://www.science.org/doi/pdf/10.1126/science.ady4652>.

[32] M. Calamai, A. Ranfagni, and F. Marin, Transfer of a levitating nanoparticle between optical tweezers, *AIP Advances* **11**, 025246 (2021), <https://doi.org/10.1063/5.0024432>.

[33] V. Vuletić and S. Chu, Laser cooling of atoms, ions, or molecules by coherent scattering, *Phys. Rev. Lett.* **84**, 3787 (2000).

[34] D. Windey, C. Gonzalez-Ballester, P. Maurer, L. Novotny, O. Romero-Isart, and R. Reimann, Cavity-based 3d cooling of a levitated nanoparticle via coherent scattering, *Phys. Rev. Lett.* **122**, 123601 (2019).

[35] U. Delić, M. Reisenbauer, D. Grass, N. Kiesel, V. Vuletic, and M. Aspelmeyer, Cavity cooling of a levitated nanosphere by coherent scattering, *Physical Review Letters* **122**, 123602 (2019).

[36] M. Toroš and T. S. Monteiro, Quantum sensing and cooling in three-dimensional levitated cavity optomechanics, *Phys. Rev. Research* **2**, 023228 (2020).

[37] M. Toroš, U. c. v. Delić, F. Hales, and T. S. Monteiro, Coherent-scattering two-dimensional cooling in levitated cavity optomechanics, *Phys. Rev. Research* **3**, 023071 (2021).

[38] K. Børkje and F. Marin, Quantum state purity versus average phonon number for characterization of mechanical oscillators in cavity optomechanics, *Phys. Rev. A* **107**, 013502 (2023).

[39] W. Bowen and G. Milburn, *Quantum Optomechanics* (CRC Press, 2015).

- [40] L.-M. Duan, G. Giedke, J. I. Cirac, and P. Zoller, Inseparability criterion for continuous variable systems, *Phys. Rev. Lett.* **84**, 2722 (2000).
- [41] R. Simon, Peres-horodecki separability criterion for continuous variable systems, *Phys. Rev. Lett.* **84**, 2726 (2000).
- [42] G. Vidal and R. F. Werner, Computable measure of entanglement, *Phys. Rev. A* **65**, 032314 (2002).
- [43] M. B. Plenio, Logarithmic negativity: A full entanglement monotone that is not convex, *Phys. Rev. Lett.* **95**, 090503 (2005).
- [44] A. Pontin, H. Fu, M. Toroš, T. S. Monteiro, and P. F. Barker, Simultaneous cavity cooling of all six degrees of freedom of a levitated nanoparticle, *Nature Physics* **19**, 1003–1008 (2023).
- [45] M. Kamba, R. Shimizu, and K. Shimizu, Nanoscale feedback control of six degrees of freedom of a near-sphere, *Nat Commun* **14**, 7943 (2023).
- [46] L. Dania, O. S. Kremer, J. Piotrowski, D. Candoli, J. Vijayan, O. Romero-Isart, C. Gonzalez-Ballester, L. Novotny, and M. Frimmer, High-purity quantum optomechanics at room temperature, *Nature Physics* **21**, 1603–1608 (2025).
- [47] M. Rademacher, A. Pontin, J. M. H. Gosling, P. F. Barker, and M. Toroš, *Roto-translational optomechanics* (2025).
- [48] J. Vijayan, J. Piotrowski, C. Gonzalez-Ballester, K. Weber, O. Romero-Isart, and L. Novotny, Cavity-mediated long-range interactions in levitated optomechanics, *Nature Physics* **20**, 859 (2024).
- [49] A. Pontin, Q. Deplano, A. Ranfagni, F. Marino, and F. Marin, Strong coupling and dark modes in the motion of a pair of levitated nanoparticles, *Phys. Rev. Lett.* **135**, 073602 (2025).
- [50] A. K. Chauhan, O. Černotík, and R. Filip, Tuneable gaussian entanglement in levitated nanoparticle arrays, *npj Quantum Information* **8**, 151 (2022).
- [51] S. Bose, A. Mazumdar, G. W. Morley, H. Ulbricht, M. Toroš, M. Paternostro, A. A. Geraci, P. F. Barker, M. S. Kim, and G. Milburn, Spin entanglement witness for quantum gravity, *Phys. Rev. Lett.* **119**, 240401 (2017).
- [52] C. Marletto and V. Vedral, Gravitationally induced entanglement between two massive particles is sufficient evidence of quantum effects in gravity, *Phys. Rev. Lett.* **119**, 240402 (2017).